Materials Advances

PAPER

View Article Online
View Journal | View Issue

Cite this: *Mater. Adv.*, 2021, 2, 3328

Synthesis and superconductivity of new TiNiSi-type equiatomic germanide ThIrGe

Guorui Xiao,[abc] Qinqing Zhu,[bcd] Yanwei Cui,[abc] Bin Liu,[bc] Jifeng Wu,[bc] Baizhuo Li,[a] Siqi Wu,[a] Guang-han Cao[a] and Zhi Ren *[bc]

Received 22nd February 2021,
Accepted 10th April 2021

DOI: 10.1039/d1ma00154j

rsc.li/materials-advances

A new germanide ThIrGe has been synthesized and characterized by X-ray diffraction, transmission electron microscopy, electrical resistivity, magnetic susceptibility and thermodynamic measurements. The structural refinement shows that, in contrast to tetragonal ThIrSi, ThIrGe crystallizes in the TiNiSi-type orthorhombic structure with the *Pnma* space group (a = 7.2321(2) Å, b = 4.3802(1) Å, and c = 7.7107(2) Å), which is the first Th-based ternary equiatomic intermetallic compound of this structural type. Below T_c = 5.25 K, ThIrGe becomes a weak-coupling type-II superconductor with a fully isotropic superconducting gap. The Sommerfeld coefficient, upper critical field, and Ginzburg–Laudau parameter are determined to be 11.8 mJ mol^{-1} K^{-2}, 2.9 T, and 19.9, respectively. First-principles calculations indicate that the density of states at the Fermi level are dominated by a hybridized contribution from the orbitals of Th, Ir and Ge, and are enhanced by the spin–orbit coupling. In addition, we demonstrate that the structural difference between ThIrGe and ThIrSi can be understood in terms of the Gibbs formation energy.

1 Introduction

Ternary equiatomic intermetallic compounds are a large family of materials and have been studied extensively over the past few decades.[1–6] These compounds have the general formula MM′X, where M can be an early transition-metal, a rare-earth or an actinide element, M′ is a late transition-metal element, and X is Si, Ge or P. Depending on the constituent elements, the MM′X compounds crystallize in a variety of structures, including hexagonal ZrNiAl-type,[7] orthorhombic TiNiSi-type,[8] and tetragonal LaPtSi-type[9] (see Fig. 1). Both the ZrNiAl-type and TiNiSi-type structures can be viewed as two-dimensional homologues based on the AlB_2-type structure, in which the key structural component is the tricapped trigonal prisms with metal atoms at the corners and non-metal atoms in the center.[10] The ZrNiAl-type structure contains six-membered rings enclosing an isolated prism, while the TiNiSi-type one consists of zigzag sheets of corner-sharing trigonal prisms.[11] By contrast, the LaPtSi-type structure is noncentrosymmetric and an ordered variant of the α-$ThSi_2$ structure.[12] In addition to this structural diversity, these ternary compounds exhibit a range of interesting physical properties, such as complex magnetic ordering,[9,13–15] heavy fermion behavior[16,17] and superconductivity.[18–24]

Among the TiNiSi-type MM′X compounds, the U-based UTGe (T = Co, Rh and Ir) has received considerable attention. UCoGe[19,25] and URhGe[20] show coexistence of ferromagnetism and superconductivity at ambient pressure. While the underlying mechanism remains unclear, both superconductivity and magnetic order are believed to be due to the U 5f electrons. In comparison, UIrGe orders antiferromagnetically and exhibits no superconductivity.[17,26] Except for 5f electrons, Th has the same electronic configuration as U. It is thus of interest to investigate the Th-based isostructural counterparts, which serve as nonmagnetic references to UTGe. However, for the ThTGe series, only ThCoGe has been known to exist and it has an AlB_2-type structure.[27] Moreover, while all of ThTSi members can be synthesized and are found to be superconducting, they adopt the noncentrosymmetric LaPtSi-type structure.[28] Actually, to our knowledge, no Th-based ternary equiatomic compound with the TiNiSi-type structure has been reported to date.

In this paper, we report the synthesis, crystal structure and physical properties of ThIrGe, a new ternary phase in the Th–Ir–Ge system. It is found that this compound possesses the orthorhombic TiNiSi-type structure and exhibits bulk type-II superconductivity below 5.25 K, which is the highest among ternary equiatomic germanides. Various superconducting parameters such as electron–phonon coupling constant, critical fields, coherence length and penetration depth, are obtained. Theoretical calculations reveal a significant hybridization between the Th, Ir and Ge orbitals at the Fermi level and

---

[a] Department of Physics, Zhejiang University, Hangzhou 310027, P. R. China
[b] School of Science, Westlake University, 18 Shilongshan Road, Hangzhou 310064, P. R. China. E-mail: renzhi@westlake.edu.cn
[c] Institute of Natural Sciences, Westlake Institute for Advanced Study, 18 Shilongshan Road, Hangzhou 310064, P. R. China
[d] Department of Physics, Fudan University, Shanghai 200433, P. R. China

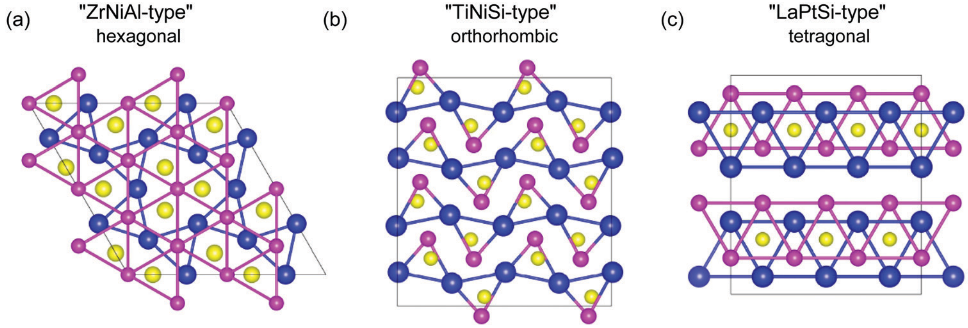

Fig. 1 Schematic structure of (a) hexagonal ZrNiAl-type, (b) orthorhombic TiNiSi-type and (c) tetragonal LaPtSi-type ternary equiatomic intermetallic compounds. The blue, pink, and yellow atoms correspond to M, M′, and X, respectively.

nonnegligible effects of spin–orbit coupling (SOC). In addition, a comparison is made between the Gibbs formation energies of ThIrGe and ThIrSi in both the TiNiSi-type and LaPtSi-type structures.

2 Materials and methods

Polycrystalline ThIrGe sample was prepared by the arc-melting method. Stoichiometric amounts of high purity Th (99.5%), Ir (99.9%) and Ge (99.99%) elements were mixed and pressured into a pellet in an argon-filled glove box. The pellet was melted in an arc furnace under high-purity argon atmosphere for several times to ensure homogeneity, followed by rapid cooling on a water-chilled copper plate. The as-cast ingot was sealed into an evacuated quartz tube, annealed at 1000 °C for 7 days, and then quenched to room temperature. The phase purity was checked by powder X-ray diffraction (XRD) at room temperature using a Bruker D8 Advance diffractometer with Cu Kα radiation. The crystal structure refinement was carried out using the Rietveld method with the GSAS software.[29] The chemical composition was measured by the Octane Plus Detector (AMETEX EDAX) coupled to a field-emitting scanning electron microscope (SEM; Hitachi S-4800). The microstructure was examined in a FEI Tecnai G2 F20 S-TWIN transmission electron microscope (TEM) operated at an accelerating voltage of 200 kV. Electrical resistivity and specific heat data were measured in a Quantum Design Physical Property Measurement System (PPMS-9 Dynacool). The dc magnetization measurements were performed in a Quantum Design Magnetic Property Measurement System (MPMS3).

First-principles calculations were carried out in the Vienna Ab initio Simulation Package (VASP)[30] based on density functional theory. The Perdew–Burke–Ernzerhof (PBE)[31] exchange–correlation functional was used and the convergence threshold of Hellmann–Feynman force is 0.01 eV Å^{-1}. The energy convergence criterion was set to 10^{-6} eV for structural optimization and 10^{-8} eV for other purposes. In both structural optimization and self-consistent calculations, the wavefunction cutoff energy was fixed to 450 eV and the Γ-centered $\boldsymbol{k}$ mesh was set to 5 × 8 × 4. The latter was increased to 10 × 16 × 8 for density-of-state (DOS) calculations.

3 Results and discussion

3.1 Crystal structure and chemical composition

Fig. 2 shows XRD patterns of ThIrGe together with its structural refinement profile, and the refined results are listed in Table 1.

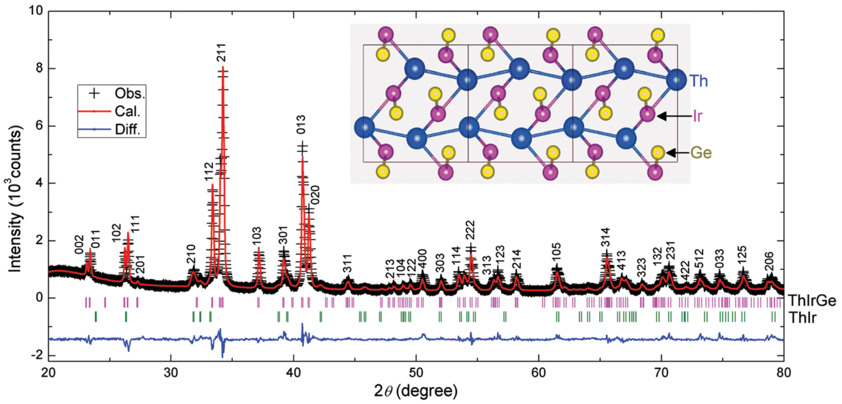

Fig. 2 Powder X-ray diffraction pattern at room temperature together with its structural refinement profile for the ThIrGe sample. The black crosses are the observed patterns and indexed on an orthorhombic unit-cell. The red and blue lines are the calculated pattern and difference plot, respectively. The peak positions for ThIrGe and ThIr are indicated by the ticks. The inset shows a schematic structure of ThIrGe, and the bonds between nearest-neighbour Th–Th, Th–Ir and Ir–Ge atoms are highlighted.

Except for a few small ones, the diffraction peaks can be well indexed on an orthorhombic lattice with the *Pnma* space group. This indicates that the main phase of the sample has a TiNiSi-type structure, which is used for the structural refinement. There is a satisfactory agreement between the calculated and observed patterns ($R_{\mathrm{wp}} = 6.5\%$, $R_{\mathrm{p}} = 4.9\%$, $\chi^2 = 2.45$) and a minor impurity phase of ThIr ($\sim$8%) is also identified. The refined lattice parameters are a = 7.2321(2) Å, b = 4.3802(1) Å, c = 7.7107(2) Å, which yields a unit-cell volume of 244.26(2) Å^3. In the lattice of ThIrGe, all of Th, Ir and Ge atoms occupy the (0.0098, 0.25, 0.7024), (0.2864, 0.25, 0.4121) and (0.1864, 0.25, 0.0816), respectively, all of which are locally non-centrosymmetric. As shown in the inset of Fig. 2, the nearest neighbour Th atoms form zigzag chains running along the a-axis with an interatomic distance of 3.689 Å, which is slightly larger than that (3.60 Å) of the sum of thorium atomic radii. A set of selected interatomic distances in ThIrGe structure is given in Table 2. One can note that the nearest neighbour distance between the Th and Ir atom is only 3.002 Å. Actually, this Th-Ir distance is even shorter than those of in the cubic Lave phase superconductor $\mathrm{ThIr_2}$ (3.176 Å)[32] and noncentrosymmetric superconductor ThIrSi (3.138 Å).[28] This, together with the short nearest neighbour Th–Ir (3.002 Å), and Ir–Ge (2.557 Å) distances, suggests a hybridization of Th, Ir and Ge orbitals at the Fermi level, which is consistent with the theoretical calculation results shown below.

This crystal structure of ThIrGe is further confirmed by high-resolution TEM (HRTEM) measurements on single-crystalline grains, typical results of which are displayed in Fig. 3(a) and (b). As can be seen in Fig. 3(a), the selected-area electron diffraction (SAED) taken along [−2 1 1] zone axis exhibits a well-defined spot pattern, and the spots near the center can be indexed to the (102), (111) and (213) planes of the TiNiSi-type structure. Moreover, from the HRTEM image of the same area shown in Fig. 3(b), two lattice spacings of 0.327 nm and 0.340 nm can be resolved, which correspond well to the (111) and (102) planes, respectively. Note that the angle between these planes is 53°, which is quite as expected in the TiNiSi-type structure. On the other hand, the EDX measurements show that the ThIrGe sample is chemically homogeneous with an average composition of $\mathrm{Th_{0.9(1)}IrGe_{1.1(1)}}$. This demonstrates that ThIrGe is stoichiometric within the experimental error, in agreement with the refined occupancies.

Table 1 Structural refinement results for ThIrGe

ThIrGe					
Space group					*Pnma*
a (Å)					7.2321(2)
b (Å)					4.3802(1)
c (Å)					7.7107(2)
V (Å^3)					244.26(2)
R_{wp}					6.5%
R_{p}					4.9%
χ^2					2.45
Atoms	X	y	z	Occ.	U_{iso}
Th	0.0098(5)	0.25	0.7024(1)	1	0.0064(6)
Ir	0.2864(4)	0.25	0.4121(3)	1	0.0075(1)
Ge	0.1864(7)	0.25	0.0816(7)	1	0.021(2)

Table 2 Selected interatomic distances for ThIrGe

Interaction	Distance (Å)	Interaction	Distance (Å)
Th–Ge (×2)	3.238(5)	Th–Th (×2)	3.816(2)
Th–Ge (×2)	3.096(5)	Th–Th (×2)	3.689(1)
Th–Ge (×1)	3.190(6)	Th–Ir (×1)	3.002(4)
Th–Ge (×1)	3.205(6)	Th–Ir (×1)	3.382(4)
Ir–Ge (×1)	2.649(5)	Th–Ir (×2)	3.189(3)
Ir–Ge (×1)	2.894(5)	Th–Ir (×2)	3.095(3)
Ir–Ge (×2)	2.557(2)		

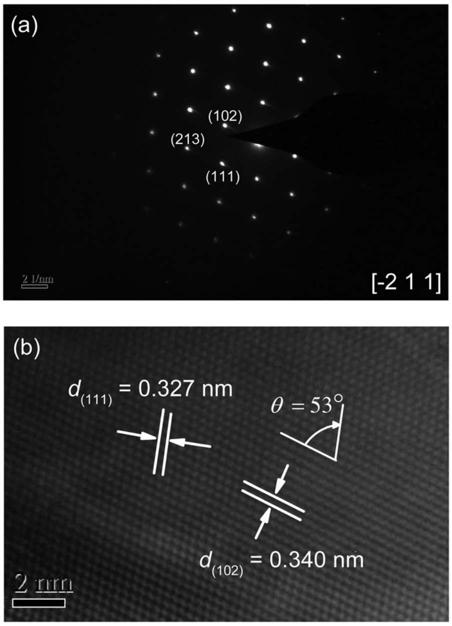

Fig. 3 (a) Selected-area electron diffraction pattern taken along the [−2 1 1] zone axis of a single-crystalline grain of the ThIrGe sample. (b) The corresponding high resolution TEM image. The distance and angel between the planes are indicated.

3.2 Normal-state and superconducting properties

The temperature dependence of resistivity ρ under zero field for the ThIrGe sample is shown in Fig. 4(a). With decreasing temperature, ρ decreases smoothly and exhibits a metallic behavior. The residual resistivity ρ_0 and residual resistivity ratio RRR = ρ(300 K)/ρ_0 are $\sim$75 μΩ cm and $\sim$3.3, respectively. Nevertheless, since our sample has a polycrystalline nature, these values depend largely on the contribution of grain boundaries and hence are not a good indicator of the sample quality. On cooling below 5.5 K, ρ drops abruptly and becomes zero at $\sim$5 K. As shown in Fig. 4(b), the resistive transition is gradually suppressed to lower temperature with increasing the magnetic field. This clearly indicates that the ρ drop is due to a superconducting transition. Here T_{c} is defined as the midpoint of ρ drop and found to be 5.25 K at zero field. While this value

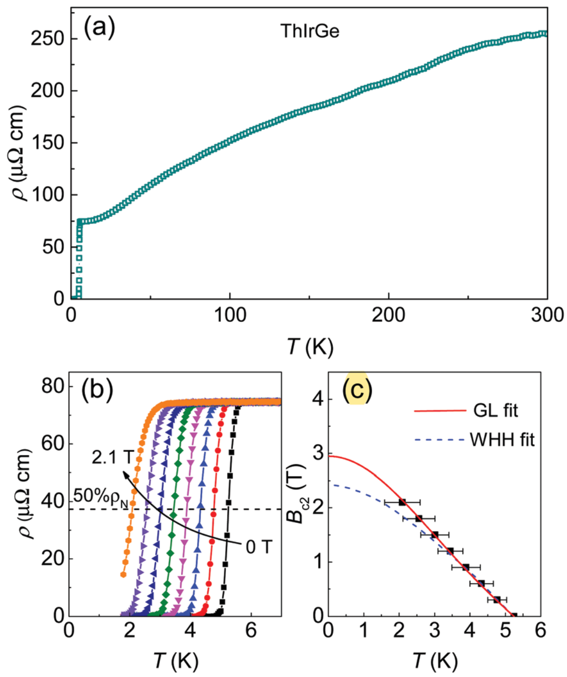

Fig. 4 (a) Temperature dependence of resistivity for the ThIrGe sample. (b) Low temperature resistivity data under various fields from 0 up to 2.1 T. (c) Temperature dependence of the upper critical field with the horizontal error bars denoting the transition width. The red solid line and blue dashed line are GL and WHH fits to the data, respectively.

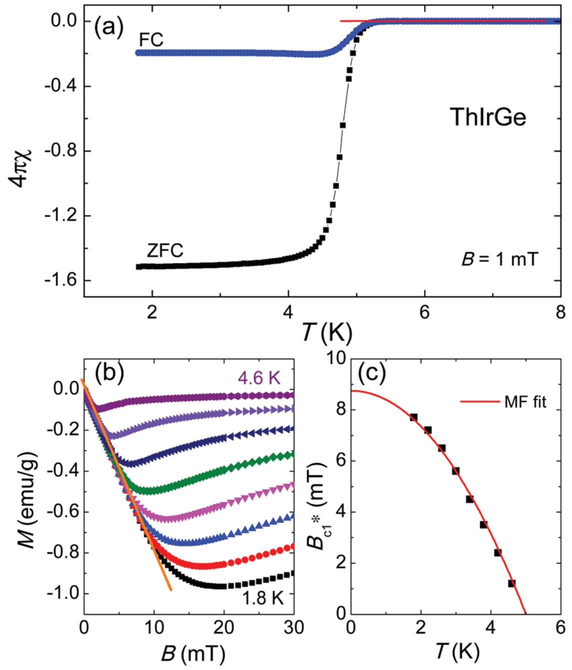

Fig. 5 (a) Low temperature magnetic susceptibility measured on the ThIrGe sample under an applied field of 1 mT. (b) Isothermal magnetization curves for the sample at various temperatures between 1.8 and 4.6 K. The solid line denotes the initial linear behavior. (c) Temperature dependence of the effective lower critical field. The solid line is a mean-field fit to the data (see text).

is close to that of $ThIr_2$ (5.58 K),[32] no corresponding phase is detected in XRD and SEM analysis. In addition, although ThIr impurity is present, its reported T_c is only 0.37 K.[33] Thus the observed superconductivity is undoubtedly ascribed to ThIrGe. To our knowledge, this T_c of 5.25 K is higher than any previously known ternary equiatomic germanides.[34] Following the same criterion at zero field, the T_c values at various fields are obtained and summarized in the upper critical field (B_{c2}) *versus* temperature phase diagram displayed in Fig. 4(c), in which the horizontal error bars denote the transition width. Notably, the B_{c2} data show deviation from the Werthamer–Helfand–Hohenberg curve[35] at low temperature but follow nicely the Ginzburg–Landau (GL) relationship

$$B_{c2}(T) = B_{c2}(0)\frac{1-t^2}{1+t^2}, \tag{1}$$

where $t = T/T_c$. An extrapolation of the data to 0 K gives the zero-temperature upper critical field $B_{c2}(0)$ = 2.9 T. This value is far below the Pauli limiting field $B_P(0) = 1.86T_c \approx 9.7$ T,[36] suggesting that B_{c2} of ThIrGe is limited by the orbital effect.

The occurrence of superconductivity in ThIrGe is corroborated by the magnetic susceptibility (χ) measurements under a magnetic field of 1 mT in both the zero-field cooling (ZFC) and field cooling (FC) modes, whose results are shown in Fig. 5(a). A strong diamagnetic transition is observed in both the ZFC and FC data, and its onset temperature of 5.22 K agrees well with the T_c determined from the resistivity measurement. Below the transition, a bifurcation develops between the two curves, which is characteristic of a type-II superconducting behavior. At 1.8 K, the χ_{ZFC} and χ_{FC} values correspond to shielding and Meissner fractions of 151.5% and 19.5%, respectively, without considering the demagnetization factor. Fig. 5(b) shows the isothermal magnetization curves at various temperatures between 1.8 and 4.6 K. In the low-field region, the $M(B)$ data decrease linearly with increasing field due to the Meissner state. At each temperature, the effective lower critical field B^*_{c1} is determined as the field at which $M(B)$ deviates from its initial linearity. The resulting temperature dependence of B^*_{c1} is displayed in Fig. 5(c) and can be well fitted by the mean-field equation:[32]

$$B^*_{c1}(T) = B^*_{c1}(0)\left[1-\left(\frac{T}{T_c}\right)^2\right], \tag{2}$$

where $B^*_{c1}(0) = 8.8$ mT is the effective zero-temperature lower critical field. Since the demagnetization factor N_d is related to the slope of initial magnetization curve through the relation

$$\mathrm{d}M/\mathrm{d}B = -\frac{1}{4\pi(1-N_d)}, \tag{3}$$

which gives N_d = 0.31. Then the zero-temperature lower critical field $B_{c1}(0)$ is calculated to be $B^*_{c1}(0)/(1-N_d) = 12.8$ mT. In addition, the shielding and Meissner fractions after demagnetization correction are 104.5% and 13.5%, respectively, suggesting that superconductivity occurs in almost the whole sample volume.

With the values of $B_{c1}(0)$ and $B_{c2}(0)$, various superconducting parameters can be determined. First, the Ginzburg-Landau coherence length $\xi_{GL}(0)$ is calculated to be 107 Å using the formula

$$\xi_{GL}(0) = \sqrt{\frac{\Phi_0}{2\pi B_{c2}(0)}}, \tag{4}$$

where $\Phi_0 = 2.07 \times 10^{-15}$ Wb is the flux quantum. Second, the GL parameter κ_{GL} can be derived from the equation[37]

$$\frac{B_{c1}(0)}{B_{c2}(0)} = \frac{\ln \kappa_{GL} + 0.5}{2{\kappa_{GL}}^2}. \tag{5}$$

This gives κ_{GL} value of 19.9, confirming that ThIrGe is a moderate type-II superconductor. Third, the penetration depth λ_{eff} is obtained from the formula

$$B_{c1}(0) = \frac{\Phi_0}{4\pi{\lambda_{eff}}^2}(\ln \kappa_{GL} + 0.5), \tag{6}$$

which yields λ_{eff} = 2120 Å.

Table 3 Normal-state and superconducting parameters of ThIrGe

Parameter	Unit	ThIrGe
T_c	K	5.25
$B_{c1}(0)$	mT	12.8
$B_{c2}(0)$	T	2.9
$\xi_{GL}(0)$	Å	107
λ_{GL}	Å	2120
κ_{GL}	—	19.9
γ	mJ mol^{-1} K^{-2}	11.8
β	mJ mol^{-1} K^{-4}	0.29
Θ_D	K	275
$\Delta C/\gamma T_c$	—	1.37
λ_{ep}	—	0.65

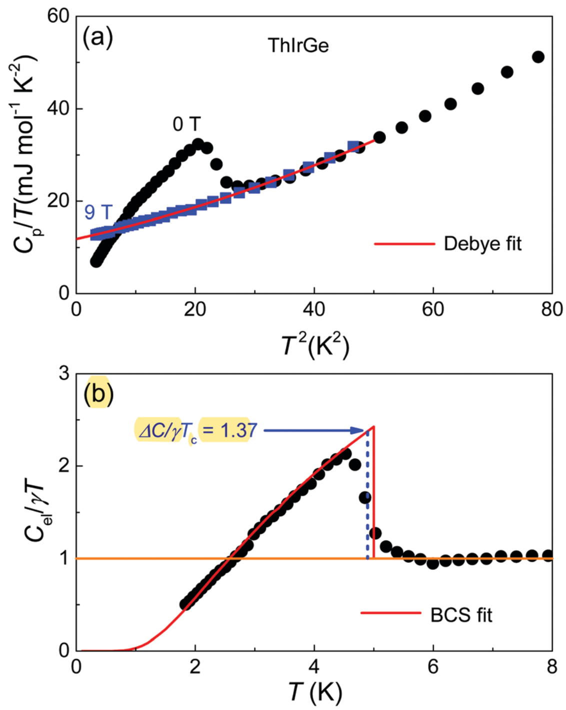

Fig. 6 (a) Low-temperature C_p/T data measured under 0 and 9 T plotted as a function of T^2 for the ThIrGe sample. The red solid line is a Debye fit to the data. (b) Temperature dependence of normalized electronic specific heat at 0 T. The red solid line is the theoretical curve from the weak coupling BCS theory. The blue dashed line and arrow demonstrate the specific heat jump $\Delta C/\gamma T_c$ value based on entropy conserving construction.

The bulk nature of superconductivity in ThIrGe is confirmed by the specific heat measurements. Fig. 6(a) shows the low-temperature specific heat (C_p) results at zero field and 9 T plotted as C_p/T *versus* T^2. The zero-filed C_p data shows a distinct jump below 5.20 K, which is very close to T_c. This anomaly is suppressed completely under 9 T, which allows us to analysis the normal-state data by the Debye model

$$C_p/T = \gamma + \beta T^2 + \delta T^4, \tag{7}$$

where γ is the Sommerfeld coefficient and $\beta(\delta)$ is the phonon specific-heat coefficient. The best fit yields γ = 11.8 mJ mol^{-1} K^{-2}, β = 0.29 mJ mol^{-1} K^{-4}, and δ = 0.0027 mJ mol^{-1} K^{-6}. Then the Debye temperature Θ_D is calculated to be 275 K using the equation

$$\Theta_D = (12\pi^4 NR/5\beta)^{1/3}, \tag{8}$$

where N = 3 is the number of atoms in the formula and R = 8.314 J mol^{-1} K^{-1} is the molar gas constant. Once Θ_D is known, the electron–phonon coupling strength λ_{ep} is estimated to 0.65 based on the inverted McMillan formula[38]

$$\lambda_{ep} = \frac{1.04 + \mu^* \ln(\Theta_D/1.45T_c)}{(1 - 0.62\mu^*)\ln(\Theta_D/1.45T_c) - 1.04}, \tag{9}$$

where μ^* = 0.13 is the Coulomb repulsion pseudopotential. Using the formula

$$N(0) = \frac{3\gamma}{\pi^2 {k_B}^2 (1 + \lambda_{ep})}, \tag{10}$$

the bare density of states at the Fermi level $N(0)$ is found to be 3.04 states eV^{-1} f.u.$^{-1}$. After subtraction of the phonon contribution, the normalized electronic specific heat $C_{el}/\gamma T$ is shown in Fig. 6(b). The entropy conversing construction of the C_p anomaly (blue dashed line) yields $\Delta C/\gamma T$ = 1.37, close to the BCS value of 1.43.[39] Indeed, The temperature dependence of $C_{el}/\gamma T$ below the peak is well reproduced by the BCS theory with a zero-temperature gap value $\Delta(0)$ = 0.73 meV (red solid line). This, together with the magnitude of λ_{ep}, implies that ThIrGe is a fully gapped *s*-wave superconductor in the weak coupling regime. The obtained normal-state and superconducting parameters are listed in Table 3.

3.3 Electronic band structure

Fig. 7(a) shows the electronic band structure for ThIrGe based on first-principles calculations both without and with SOC. In the absence of SOC, there are multiple bands crossing the Fermi level (E_F), consistent with the metallic nature of this material. Turning on the SOC results in a significant change in the band dispersion near E_F. In particular, the SOC splitting

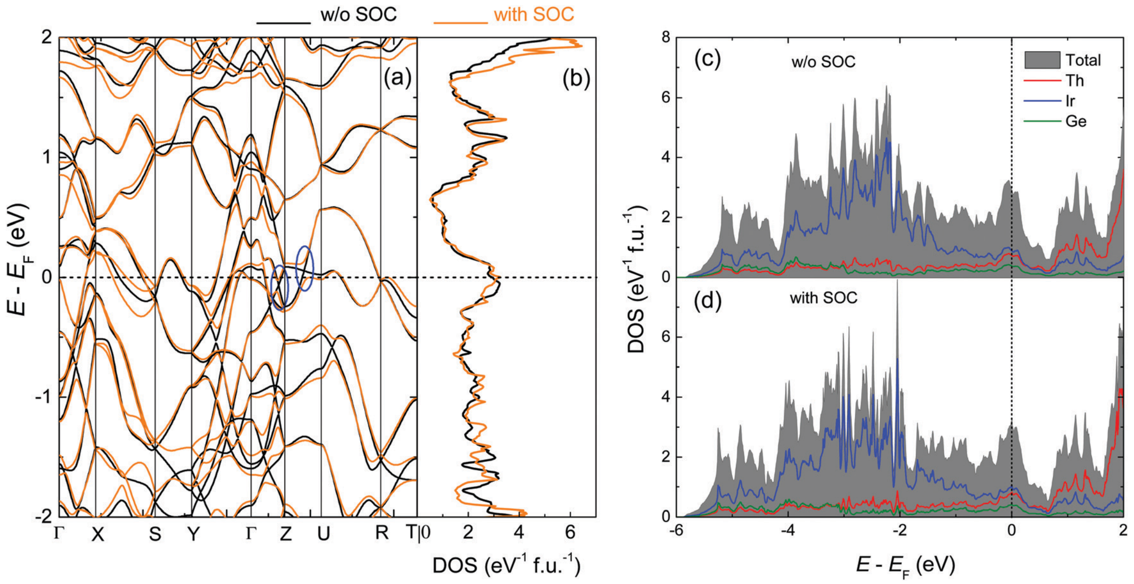

Fig. 7 (a) The electronic band structure of ThIrGe without (black) and with (orange) SOC. (b) Corresponding total density of states plotted as a function of energy. The horizontal dashed line indicates the position of Fermi level. (c and d) The projected density of states for ThIrGe without and with SOC, respectively. The vertical dashed line indicates the position of Fermi level.

reaches about 0.16 eV, and 0.17 eV along Γ–Z and Z–U lines, respectively. As a consequence, the theoretical $N(0)$ increases from 2.91 states eV^{-1} f.u.$^{-1}$ without SOC to 3.22 states eV^{-1} f.u.$^{-1}$ after switching on SOC, as seen in Fig. 7(b). While the $N(0)$ from C_p measurement lies between these two values, it is obviously larger than the one without SOC, suggesting that the DOS at E_F is indeed enhanced by the SOC. The projected DOS on atomic orbitals without and with SOC are displayed in Fig. 7(c) and (d), respectively. In both cases, the DOS for $E - E_F$ between −4 and −1 eV are dominated by the 5d orbital of Ir atoms. Nevertheless, as E moves closer to E_F, the hybridization between the orbitals of Th, Ir and Ge becomes significant. At E_F, the contribution of Th orbitals is nearly equal to that of Ir orbitals and twice that of the Ge orbitals. In the E range of 0.5 to 2 eV above E_F, the contribution form Th orbitals dominates over that from Ir orbitals while the contribution from Ge orbitals is diminished. These results clearly indicate that ThIrGe is a multiorbital system with nonnegligile spin–orbit interaction.

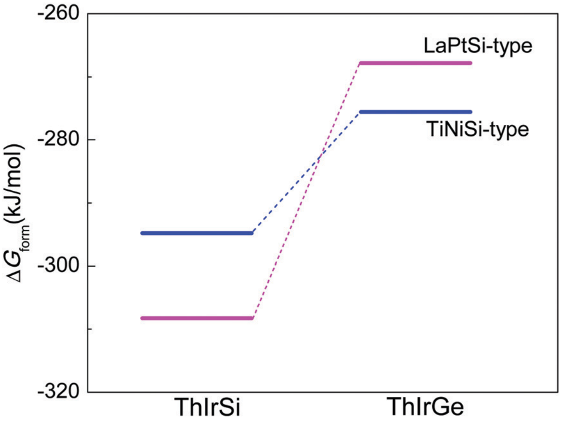

Fig. 8 The Gibbs formation energies for ThIrSi and ThIrGe in both the TiNiSi-type and LaPtSi-type structures. The two dashed lines are a guide to the eyes.

3.4 Comparison between the Gibbs formation energies of ThIrGe and ThIrSi

From the above results, it is clear that while ThIrGe is isoelectronic to ThIrSi, their crystal structures are very different. To gain insight into this issue, we examine the Gibbs formation energy ΔG_{form} of these compounds in both the TiNiSi-type and LaPtSi-type structures according to the following reaction:

$$\text{Th(s)} + \text{Ir(s)} + \text{Si(Ge)(s)} \rightarrow \text{ThIrSi(Ge)(s)}. \tag{11}$$

Here ΔG_{form} is obtained by evaluating the free-energy differences between the subsystems involved in the reaction, which is expressed as[40]

$$\Delta G_{\text{form}} = G[\text{ThIrSi(Ge)}] - G[\text{Th}] - G[\text{Ir}] - G[\text{Si(Ge)}], \tag{12}$$

where G is the free energy of each subsystem. Since we deal with bulk samples, the entropy and zero-point energy effects are neglected[41] and G can be estimated from first principles calculations. The obtained ΔG_{form} values are summarized in Fig. 8 for better elucidation. As can be seen, $\Delta G_{\text{form}} = -308.3$ kJ mol^{-1} for ThIrSi in the LaPtSi-type structure, which is lower than that of −294.8 kJ mol^{-1} in TiNiSi-type structure. The situation is opposite for ThIrGe, where ΔG_{form} is lower in the TiNiSi-type structure (−275.6 kJ mol^{-1}) than in the LaPtSi-type structure (−267.8 kJ mol^{-1}). These results indicate that ThIrSi and ThIrGe are energetically more stable in the LaPtSi-type and TiNiSi-type structures, respectively, in excellent agreement with the experimental observation. In this respect, it is of future interest to see whether ΔG_{form} can be generally applicable to predict the crystal structure of MM′X compounds.

4 Conclusions

In summary, we have synthesized and characterized a new intermetallic germanide ThIrGe. Structural analyses indicate that this compound adopts the orthorhombic TiNiSi-type structure, which is the first example of this structural type for Th-based ternary equiatomic intermetallics. Furthermore, ThIrGe is discovered to be a bulk type-II superconductor below 5.25 K with a BCS-like superconducting gap. Theoretical calculations reveal that a notable hybridization between the Th, Ir and Ge orbitals is present at the Fermi level and the corresponding density of states are enhanced by the spin–orbit interaction. In addition, we show that the structural difference between ThIrGe and ThIrSi is consistent with comparison between the Gibbs formation energy of these materials in both structures. Our results not only provide an isostructural nonmagnetic reference to UIrGe, but also help to better understand both the structural and superconducting behavior in the family of ternary equiatomic compounds.

Conflicts of interest

The authors declare no competing interests.

Acknowledgements

We acknowledge financial support by the foundation of Westlake University. The work at Zhejiang University is supported by National Key Research Development Program of China (No. 2017YFA0303002).

Notes and references

1 V. Johnson and W. Jeitschko, Ternary equiatomic transition metal silicides and germanides, *J. Solid State Chem.*, 1972, **4**, 123–130.

2 E. Hovestreydt, N. Engel, K. Klepp, B. Chabot and E. Parthe, Equiatomic ternary rare earth-transition metal silicides, germanides and gallides, *J. Less-Common Met.*, 1982, **85**, 247–274.

3 R. Muller, R. Shelton, J. Richardson Jr and R. Jacobson, Superconductivity and crystal structure of a new class of ternary transition metal phosphides TT/t′P (T = V, Zr, Nb, Ta and T/t′ = V, Ru, Rh), *J. Less-Common Met.*, 1983, **92**, 177–183.

4 G. S. Rao, K. Wagner, G. Balakrishnan, J. Janaki, W. Paulus, R. Schollhorn, V. Subramanian and U. Poppe, Structure and superconductivity studies on ternary equiatomic silicides, MM′Si, *Mater. Sci. Bull.*, 1985, **7**, 215–228.

5 F. Canepa, P. Manfrinetti, M. Pani and A. Palenzona, Structural and transport properties of some UTX compounds where T = Fe, Co, Ni and X = Si, Ge, *J. Alloys Compd.*, 1996, **234**, 225–230.

6 P. R. Zhang, H. Q. Yuan and C. Cao, Electron-phonon coupling and nontrivial band topology in noncentrosymmetric superconductors LaNiSi, LaPtSi, and LaPtGe, *Phys. Rev. B*, 2020, **101**, 245145.

7 L. Havela, M. Divis, V. Sechovsky, A. Andreev, F. Honda, G. Oomi, Y. Meresse and S. Heathman, U ternaries with ZrNiAl structure-Lattice properties, *J. Alloys Compd.*, 2001, **322**, 7–13.

8 G. A. Landrum, R. Hoffmann, J. Evers and H. Boysen, The TiNiSi family of compounds: structure and bonding, *Inorg. Chem.*, 1998, **37**, 5754–5763.

9 S. Ramakrishnan, K. Ghosh, A. D. Chinchure, V. Marathe and G. Chandra, Magnetism and superconductivity in RPtSi (R = La, Ce, Nd, and Sm), *Phys. Rev. B: Condens. Matter Mater. Phys.*, 1995, **52**, 6784.

10 A. O. Oliynyk, L. A. Adutwum, B. W. Rudyk, H. Pisavadia, S. Lotfi, V. Hlukhyy, J. J. Harynuk, A. Mar and J. Brgoch, Disentangling structural confusion through machine learning: structure prediction and polymorphism of equiatomic ternary phases ABC, *J. Am. Chem. Soc.*, 2017, **139**, 17870–17881.

11 G. J. Miller and J. Cheng, Ternary Metal-Rich Phosphides: Structure, Bonding, and Site Preferences in ZrNbP and $Hf_{1+x}Mo_{1-x}P$, *Inorg. Chem.*, 1995, **34**, 2962–2968.

12 K. Klepp and E. Parthe, RPtSi phases (R = La, Ce, Pr, Nd, Sm and Gd) with an ordered $ThSi_2$ derivative structure, *Acta Crystallogr., Sect. B: Struct. Crystallogr. Cryst. Chem.*, 1982, **38**, 1105–1108.

13 R. Troc and V. Tran, Magnetic properties of UT(Si,Ge) series, *J. Magn. Magn. Mater.*, 1988, **73**, 389–397.

14 T. Ueda, D. Honda, T. Shiromoto, N. Metoki, F. Honda, K. Kaneko, Y. Haga, T. D. Matsuda, T. Takeuchi, A. Thamizhavel, K. Sugiyama, K. Kindo, R. Settai and Y. Onuki, Magnetic property and pressure effect of a single crystal CeRhGe, *J. Phys. Soc. Jpn.*, 2005, **74**, 2836–2842.

15 F. Kneidinger, I. Zeiringer, A. Siderenko, E. Bauer, H. Michor, P. Rogl and J. Sereni, Physical properties of CeIrSi with trillium-lattice frustrated magnetism, *Phys. Rev. B*, 2019, **100**, 134442.

16 W. Lee and R. Shelton, CePtSi: a new heavy-fermion compound, *Phys. Rev. B: Condens. Matter Mater. Phys.*, 1987, **35**, 5369.

17 A. Ramirez, B. Batlogg and E. Bucher, Magnetothermal properties of UIrGe and systematic trends in magnetic heavy fermion compounds, *J. Appl. Phys.*, 1987, **61**, 3189–3190.

18 W. Lee, F. Yang, C. Shih and H. Yang, Crystal structure and superconductivity in the Ni-based ternary compound LaNiSi, *Phys. Rev. B: Condens. Matter Mater. Phys.*, 1994, **50**, 6523.

19 N. Huy, A. Gasparini, D. De Nijs, Y. Huang, J. Klaasse, T. Gortenmulder, A. de Visser, A. Hamann, T. Gorlach and H. V. Lohneysen, Superconductivity on the border of weak itinerant ferromagnetism in UCoGe, *Phys. Rev. Lett.*, 2007, **99**, 067006.

20 D. Aoki, A. Huxley, E. Ressouche, D. Braithwaite, J. Flouquet, J.-P. Brison, E. Lhotel and C. Paulsen, Coexistence of

superconductivity and ferromagnetism in URhGe, *Nature*, 2001, **413**, 613–616.

21 Y. P. Qi, J. G. Guo, H. C. Lei, Z. W. Xiao, T. Kamiya and H. Hosono, Superconductivity in noncentrosymmetric ternary equiatomic pnictides LaMP (M = Ir and Rh; P = P and As), *Phys. Rev. B: Condens. Matter Mater. Phys.*, 2014, **89**, 024517.

22 Y. Okamoto, T. Inohara, Y. Yamakawa, A. Yamakage and K. Takenaka, Superconductivity in the hexagonal ternary phosphide ScIrP, *J. Phys. Soc. Jpn.*, 2016, **85**, 013704.

23 K. Domieracki and D. Kaczorowski, Superconductivity in a non-centrosymmetric compound ThCoSi, *J. Alloys Compd.*, 2016, **688**, 206–210.

24 D. Singh, P. Biswas, A. Hillier and R. Singh, *et al.*, Superconducting properties of the noncentrosymmetric superconductor LaPtGe, *Phys. Rev. B*, 2018, **98**, 214505.

25 T. Hattori, Y. Ihara, Y. Nakai, K. Ishida, Y. Tada, S. Fujimoto, N. Kawakami, E. Osaki, K. Deguchi, N. Sato and I. Satoh, Superconductivity induced by longitudinal ferromagnetic fluctuations in UCoGe, *Phys. Rev. Lett.*, 2012, **108**, 066403.

26 B. Chevalier, B. Lloret, P. Gravereau, B. Buffat and J. Etourneau, Kondo fluctuations and magnetism in the new equiatomic ternary compounds UIrSi and UIrGe, *J. Magn. Magn. Mater.*, 1988, **75**, 13–18.

27 P. Manfrinetti, A. Palenzona, S. Dhar and C. Mitra, Structure and properties of some new Th compounds, *Intermetallics*, 1999, **7**, 1291–1294.

28 A. Ptok, K. Domieracki, K. Kapcia, J. Lazewski, P. Jochym, M. Sternik, P. Piekarz and D. Kaczorowski, Electronic and lattice properties of noncentrosymmetric superconductors ThTSi (T = Co, Ir, Ni, and Pt), *Phys. Rev. B*, 2019, **100**, 165130.

29 B. H. Toby, EXPGUI, a graphical user interface for GSAS, *J. Appl. Crystallogr.*, 2001, **34**, 210–213.

30 G. Kresse and J. Furthmuller, Efficiency of ab-initio total energy calculations for metals and semiconductors using a plane-wave basis set, *Comput. Mater. Sci.*, 1996, **6**, 15–50.

31 J. P. Perdew, K. Burke and M. Ernzerhof, Generalized gradient approximation made simple, *Phys. Rev. Lett.*, 1996, **77**, 3865.

32 G. R. Xiao, S. Q. Wu, B. Z. Li, B. Liu, J. F. Wu, Y. W. Cui, Q. Q. Zhu, G. H. Cao and Z. Ren, Normal-state and superconducting properties of the cubic Laves phase $ThIr_2$, *Intermetallics*, 2021, **128**, 106993.

33 T. Geballe, B. Matthias, V. Compton, E. Corenzwit, G. Hull Jr and L. D. Longinotti, Superconductivity in binary alloy systems of the rare earths and of thorium with Pt-group metals, *Phys. Rev.*, 1965, **137**, A119.

34 X. Wang, C. B. J. Etourneau and P. Hagenmuller, Crystal structure and superconductivity of new ternary MTGe germanides (M = Ti, Zr, Hf and T = Ru, Os, Rh, Ir), *Mater. Res. Bull.*, 1987, **22**, 331.

35 N. Werthamer, E. Helfand and P. Hohenberg, Temperature and purity dependence of the superconducting critical field, Hc_2. III. Electron spin and spin-orbit effects, *Phys. Rev.*, 1966, **147**, 295.

36 A. M. Clogston, Upper limit for the critical field in hard superconductors, *Phys. Rev. Lett.*, 1962, **9**, 266.

37 C.-R. Hu, Numerical constants for isolated vortices in superconductors, *Phys. Rev. B: Condens. Matter Mater. Phys.*, 1972, **6**, 1756.

38 W. McMillan, Transition temperature of strong-coupled superconductors, *Phys. Rev.*, 1968, **167**, 331.

39 J. Bardeen, L. N. Cooper and J. R. Schrieffer, Therory of Superconductivity, *Phys. Rev.*, 1957, **108**, 1175.

40 J. I. Martinez, H. A. Hansen, J. Rossmeisl and J. K. Norskov, Formation energies of rutile metal dioxides using density functional theory, *Phys. Rev. B: Condens. Matter Mater. Phys.*, 2009, **79**, 045120.

41 M. Bollinger, K. W. Jacobsen and J. K. Norskov, Atomic and electronic structure of MoS_2 nanoparticles, *Phys. Rev. B: Condens. Matter Mater. Phys.*, 2003, **67**, 085410.